

1 **Effect of a thin weak layer at around the 660-km discontinuity on subducting**  
2 **slab morphology in the mantle transition zone**

3

4 Zhong-Hai Li<sup>1</sup>, Ling Chen<sup>2,3</sup>

5 <sup>1</sup> Key Laboratory of Computational Geodynamics, College of Earth and Planetary Sciences,  
6 University of Chinese Academy of Sciences, Beijing, China

7 <sup>2</sup> State Key Laboratory of Lithospheric Evolution, Institute of Geology and Geophysics, Chinese  
8 Academy of Sciences, Beijing, China

9 <sup>3</sup> CAS Center for Excellence in Tibetan Plateau Earth Sciences, Beijing, China

10

11

12

13 **Highlights:**

14 (1) A weak layer above 660-km discontinuity, at 610-660 km, has negligible effect on  
15 the slab morphology in the mantle transition zone (MTZ).

16 (2) A weak layer beneath 660-km discontinuity, at 660-710 km, does not change the  
17 slab mode selection (penetration versus stagnation).

18 (3) A weak layer at 660-710 km contributes to sub-horizontal slab movement and  
19 flattening in MTZ in case with high resistance from lower mantle.

20

21

22 **Abstract:**

23 The subducting slab morphology in the mantle transition zone (MTZ) is strongly  
24 affected by the mantle viscosity and density variations at the 660-km discontinuity  
25 (D660). Besides the negative Clapeyron slope of phase transition and the viscosity  
26 increase, a possible thin weak layer at around D660 is proposed to play a key role in  
27 the slab stagnation, which is however not well constrained. In this study, a series of  
28 numerical models are systematically conducted, which reveal that a weak layer  
29 beneath D660 does not change the slab mode selection (penetration versus stagnation).  
30 However, it will contribute to longer slab flattening at the bottom of the MTZ, when  
31 slab sinking is strongly resisted by either the viscosity increase or a large Clapeyron  
32 slope at D660. The role of a weak layer on slab flattening is dependent on the  
33 lubrication effect that promotes sub-horizontal slab movement at the bottom of the  
34 MTZ.

35

36 **Plain Language Summary**

37 On the Earth, an oceanic plate may sink down beneath another plate into the  
38 subjacent mantle, which is called 'subduction'. The mantle is not homogeneous, but  
39 generally divided into the upper and lower mantle with different mineral phases. The  
40 boundary locates at about 660 km depth, which is characterized by the downward  
41 density and viscosity increase, as well as the possible existence of a thin weak layer.  
42 Thus the sinking slab could be strongly affected by the 660-km discontinuity (D660),  
43 resulting in variable slab morphologies as revealed by geophysical observations. A  
44 key point is about the effect of the thin weak layer on the mode selection of sinking  
45 slab. A previous modeling study proposed that the weak layer has a critical effect on  
46 slab stagnation above D660, rather than penetrating into the lower mantle. However,  
47 the current systematic models reveal that a weak layer beneath D660 does not change  
48 the slab mode selection (penetration versus stagnation), although it will contribute to  
49 sub-horizontal slab movement and longer-distance flattening at the bottom of the  
50 MTZ in case with high resistance from the lower mantle.

51

## 52 **1. Introduction**

53 The morphology and dynamics of subducting slabs are strongly controlled by the  
54 rheological structure and layering of the Earth's mantle (e.g., *Gurnis & Hager, 1988*;  
55 *Čížková et al., 2002*; *Billen, 2010*; *Agrusta et al., 2017*; *Goes et al., 2017*; *Yang et al.,*  
56 *2018*; *Li et al., 2019*), which are however not well understood. The radial viscosity  
57 profile is generally inferred from the joint inversions of glacial isostasy adjustment  
58 data, geoid anomalies, as well as constraints from mineral physics (*Hager et al., 1985*;  
59 *Forte and Peltier, 1987, 1991*; *Ricard and Bai, 1991*; *King and Masters, 1992*; *Ricard*  
60 *et al., 1993*; *Corrieu et al., 1995*; *Forte and Mitrovica, 1996*; *Lambeck et al., 1996,*  
61 *1998*; *Mitrovica and Forte, 2004*; *Steinberger and Calderwood, 2006*; *Forte et al.,*  
62 *2010*), which shows that the average viscosity of the lower mantle is 10-100 times  
63 higher than the average upper mantle viscosity (Figure S1 in the supporting  
64 information) (*Zhu, 2016*). However, it is widely debated about the rheological  
65 transition mode between the upper and lower mantle, for example, a sharp viscosity  
66 jump or a gradual viscosity increase (Figure S1).

67 Besides the rheological contrast, the phase transition at the 660-km discontinuity  
68 (D660), i.e., the bottom of the mantle transition zone (MTZ) in between the upper and  
69 lower mantle, is characterized by a negative Clapeyron slope of  $C_{660} \in [-4.0, -0.4]$   
70 MPa/K according to a number of high-pressure laboratory experiments as summarized  
71 in *Li et al. (2019)*. Many modeling studies have been conducted to investigate how a  
72 slab interacts with D660, and generally suggest that a higher Clapeyron slope  
73 contributes significantly to the stagnation of subducting slab in the MTZ (*Goes et al.,*  
74 *2017*; *Li et al., 2019*; and references therein).

75 Another key point is about a thin weak layer at around the bottom of the MTZ  
76 proposed in some of the joint inversion models (e.g., *Mitrovica and Forte, 2004*;  
77 Figure S1). The formation mechanism of this possible weak layer is still not clear,  
78 which may be caused by grain size reduction and/or superplasticity (*Karato, 2008*),  
79 the presence of water (*Tschauner et al., 2018*), or a partially molten carbonated layer  
80 (*Sun et al., 2018*). Geodynamic models have shown that a weak layer beneath D660  
81 may have a large effect on either mantle plume branching (*Liu and Leng, 2020*) or

82 subducting slab stagnation (*Mao and Zhong, 2018*).

83 The upper/lower mantle boundary, i.e. D660 characterized by strong density and  
84 viscosity variations, is thus a critical structure for mantle dynamics. The general  
85 effects of the Clapeyron slope ( $C_{660}$ ) and viscosity jump on the morphology of  
86 subducting slabs have been widely modeled and investigated; however, the influence  
87 of a possible weak layer at around this discontinuity lacks systematic studies. *Mao*  
88 *and Zhong* (2018) proposed that this weak layer plays significant roles in the slab  
89 flattening in the MTZ, by conducting a 3-D global model and further comparing their  
90 results with seismic tomographic images. However, it remains difficult to isolate the  
91 effect of the weak layer in the complex model with prescribed surface velocities and  
92 trench motions, as well as the interactions among global subduction zones. Thus, the  
93 exact role of this weak layer, as well as the mechanism of its control on slab  
94 stagnation, is still not clear. In this study, we aim to solve this problem by applying a  
95 more generic, pure dynamic subduction model, focusing on the effects of density and  
96 viscosity variations across the weak layer at around D660.

97

## 98 **2. Initial model setup**

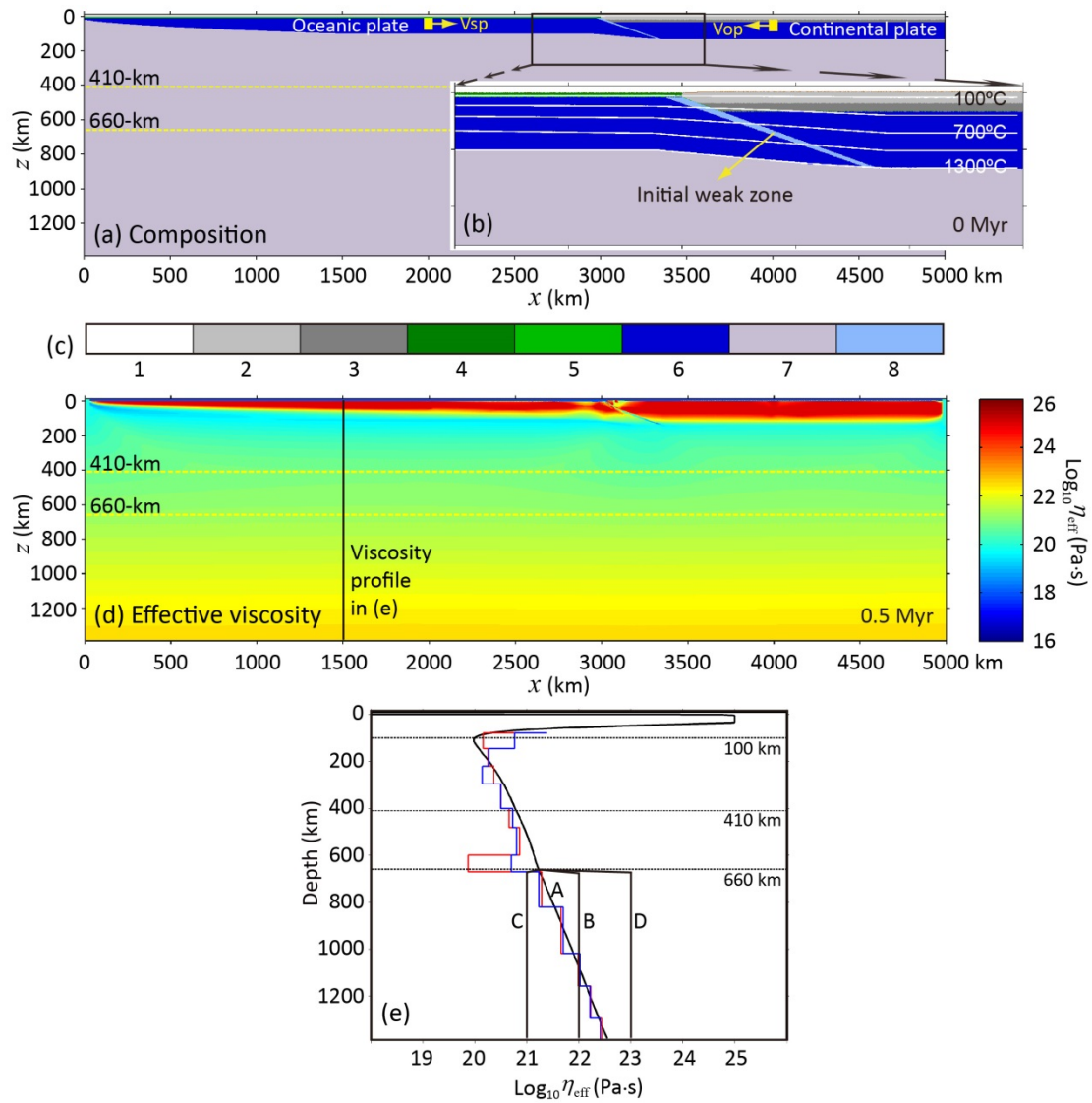
99 Numerical models are conducted with the code I2VIS (*Gerya, 2010*), which is  
100 integrated with the deep water activity and phase transitions down to 30 GPa in the  
101 deep mantle. The detailed numerical methods and implementations are shown in *Li et*  
102 *al.* (2019) and the supporting information (Text S1).

103 Large-scale numerical models are set up in a Cartesian box of  $5000 \times 1400$  km  
104 (Figure 1). In the initial model, an oceanic plate is set on the left and a continental  
105 plate on the right, with an initial weak zone in between (Figure 1a). The oceanic  
106 lithosphere includes an upper- (3 km) and a lower-crustal layer (5 km), as well as a  
107 mantle layer with the thickness dependent on the lithospheric age (60 Ma). The initial  
108 thermal structure of the oceanic lithosphere is defined by the half-space cooling model  
109 (*Turcotte and Schubert, 2002*). The continental lithosphere includes an upper crust (20  
110 km), a lower crust (15 km) and a mantle layer (100 km), with the initial thermal  
111 structure defined by a linear gradient from  $0^\circ\text{C}$  at the surface to  $1350^\circ\text{C}$  at the bottom.

112 The initial thermal gradient in the sub-lithospheric mantle is defined by a constant  
113 value of 0.5 °C/km. On the top of the model domain, a ‘sticky air’ layer with low  
114 density and viscosity is applied (*Schmeling et al., 2008; Crameri et al., 2012*).  
115 Detailed numerical parameters are shown in Tables S1 and S2 in the supporting  
116 information.

117 For the effective viscosity of multiple rock types, the composite  
118 visco-plastic-Peierls rheology is generally applied (Text S1 and Table S1). It results in  
119 a rheologically strong lithosphere and a weak asthenospheric layer beneath (Figure  
120 1d-e). Then the effective viscosity increases downward to the MTZ and lower mantle,  
121 which is generally consistent with the viscosity profiles inferred from the more recent  
122 joint observations (red and blue lines in Figure 1e) (*Mitrovica and Forte, 2004; Forte*  
123 *et al., 2010*). The effect of the weak layer at the bottom of the MTZ (Figure 1e;  
124 *Mitrovica and Forte, 2004*) or beneath the MTZ as in *Mao and Zhong (2018)* is the  
125 focus of this study and thus systematically investigated. In addition, the effect of an  
126 abrupt viscosity jump at D660 is further tested, by applying various constant  
127 viscosities in the lower mantle (Figure 1e).

128 For the boundary conditions of the model, free slip is satisfied for all boundaries.  
129 In addition, a constant convergence velocity of 5 cm/yr ( $V_{sp} = 4$  cm/yr,  $V_{op} = -1$   
130 cm/yr; Figure 1a) is applied for subduction initiation, which will be canceled after 10  
131 Myrs. For the thermal boundary conditions, fixed values of 0°C and 1975°C are  
132 applied for the top and bottom boundaries, respectively. The vertical boundaries have  
133 no horizontal heat flux.



134

135 **Figure 1.** Initial model configuration. (a) Composition field in the framework of 5000  
 136 × 1400 km, with the 410-km and 660-km discontinuities shown with yellow dashed  
 137 lines (phase transitions illustrated in Text S1 of the supporting information). (b) The  
 138 enlargement of initial subduction zone, with white lines for isotherms, starting from  
 139 100°C with the interval of 300°C. The colors in (a) and (b) indicate for rock types as  
 140 specified in (c): 1-sticky air; 2,3-continental upper and lower crust, respectively;  
 141 4,5-oceanic upper and lower crust, respectively; 6,7-lithospheric and subjacent mantle,  
 142 respectively; 8-hydrated mantle. It is worth noting that the additional rock types, e.g.,  
 143 the partially molten rocks, are not shown in the initial model, but will appear during  
 144 the evolution of the model. (d) The effective viscosity field of the model, with a  
 145 vertical profile as the A-Type shown in (e). The composite rheology is applied for  
 146 A-type (Text S1 in the supporting information), with effective viscosity increasing

147 downward in the lower mantle, which is generally consistent with the viscosity  
148 profiles inferred from the joint observations (red and blue lines) (*Mitrovica and Forte,*  
149 *2004; Forte et al., 2010*). Three additional types of numerical models are conducted  
150 with different, but constant viscosities of the lower mantle, i.e.  $10^{22}$  Pa·s (B),  $10^{21}$   
151 Pa·s (C) and  $10^{23}$  Pa·s (D), respectively.

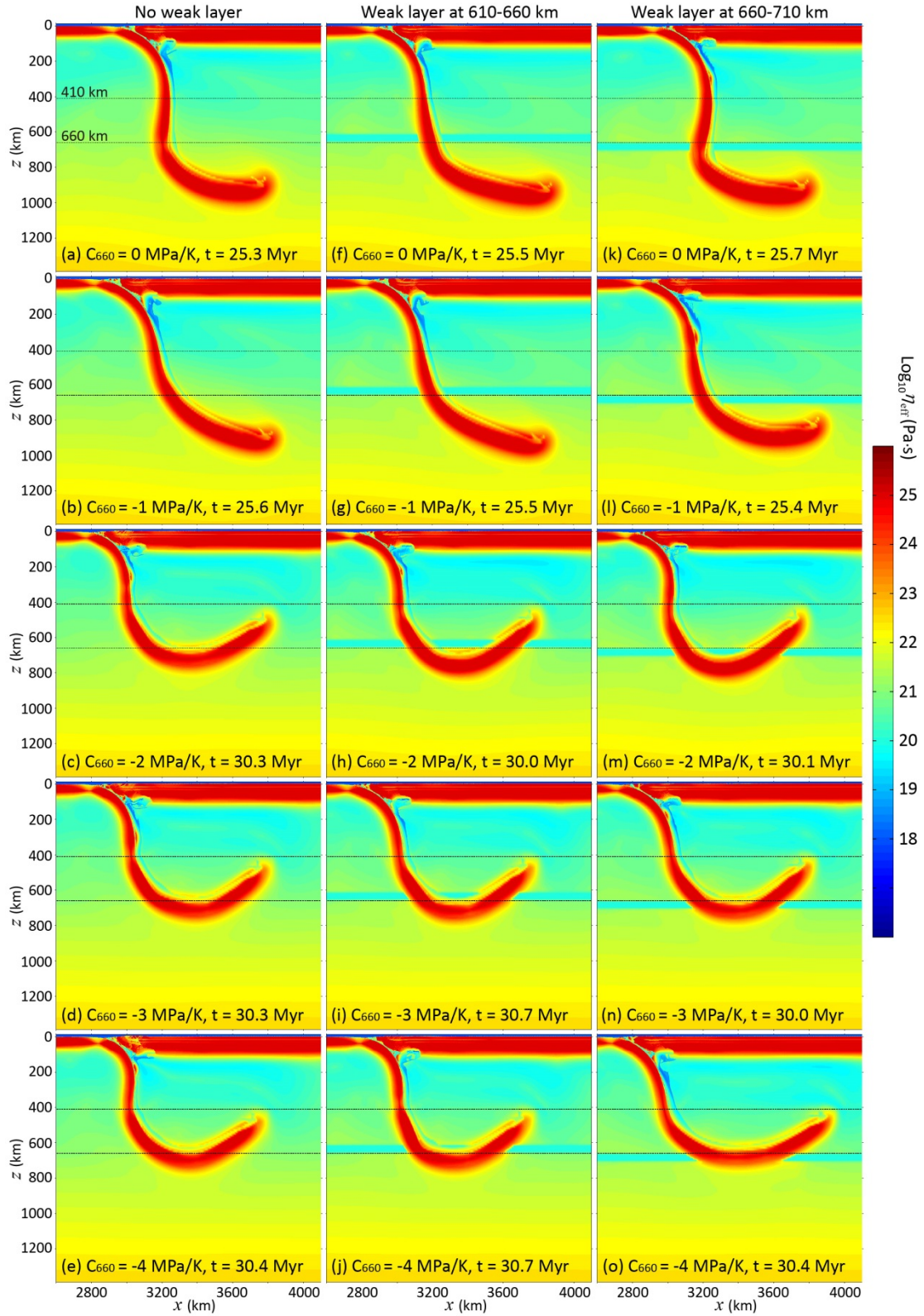
152

### 153 **3. Model results**

#### 154 **3.1. Reference models with composite rheology of the lower mantle**

155 In this section, the composite rheology is applied for all the rock types, with an  
156 effective viscosity profile (A-type) shown in Figure 1e. The effect of a weak layer is  
157 systematically studied, which is 50 km thick and has a constant viscosity of  $10^{20}$  Pa·s.  
158 The weak layer is positioned either above or beneath D660 (Figure 2), the results of  
159 which are further compared with the model without such a weak layer. In addition, the  
160 sensitivity tests with variable Clapeyron slopes at D660 are conducted.

161 The modeling and comparison results demonstrate that the existence of such a  
162 weak layer does not change the general slab mode selection between penetration and  
163 stagnation (Figure 2). In the models with a large Clapeyron slope of  $C_{660} = -4$  MPa/K,  
164 a weak layer beneath D660 can increase the length of the stagnant slab in the MTZ,  
165 comparing to the models without the weak layer or with it above D660 (c.f. Figures  
166 2e, 2j, 2o). It indicates that the weak layer beneath D660 promotes the sub-horizontal  
167 movement of the stagnant slab at the bottom of the MTZ, facilitated by the large  
168 resistance to the sinking slab due to the large negative Clapeyron slope and the  
169 resulting delay of phase transition.



170

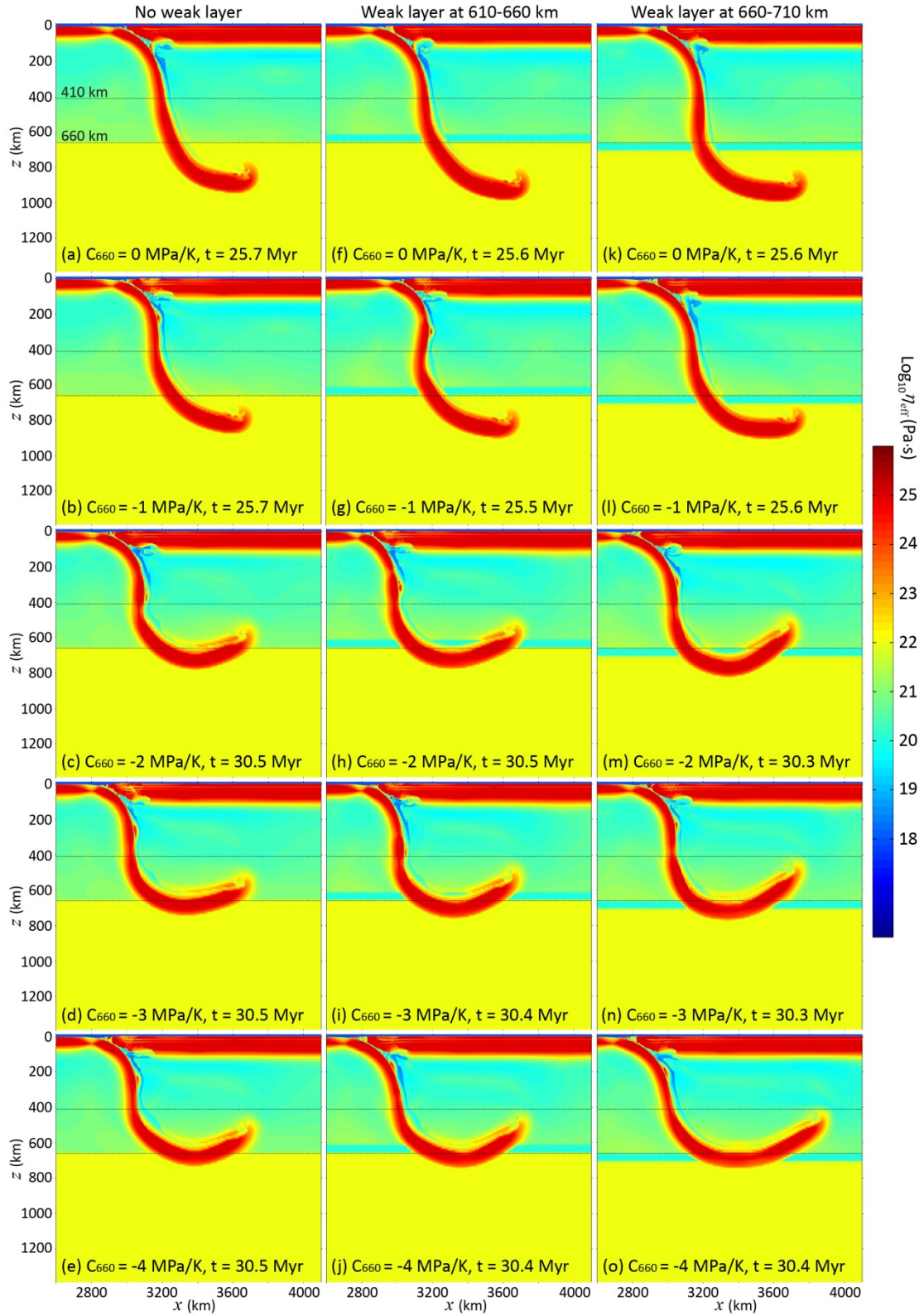
171 **Figure 2.** Model results with a composite rheological profile of the lower mantle, i.e.  
 172 A-type in Figure 1e. The effects of a thin weak layer and the Clapeyron slope ( $C_{660}$ ) at  
 173 D660 are tested.

174

175 **3.2. Models with intermediate and constant viscosity of the lower mantle ( $10^{22}$**   
176 **Pa·s)**

177 In this set of models, a constant viscosity of  $10^{22}$  Pa·s is applied for the lower  
178 mantle, with an effective viscosity profile shown in Figure 1e (B-type), which is more  
179 or less the average value of the A-type gradually increasing viscosity in the lower  
180 mantle.

181 The model results are quite similar to the ones with composite rheology of the  
182 lower mantle (c.f. Figures 3 and 2), which indicate that a sharp viscosity jump has a  
183 similar dynamic effect as an equivalent, strong viscosity-depth gradient between the  
184 lower and upper mantle. The influence of the weak layer is only obvious in the  
185 models with a high Clapeyron slope of  $C_{660} = -4$  MPa/K, which indicates again that a  
186 weak layer beneath D660 may lead to longer slab stagnation in the MTZ (c.f. Figures  
187 3e, 3j, 3o), similar to the reference models in Figure 2.



188

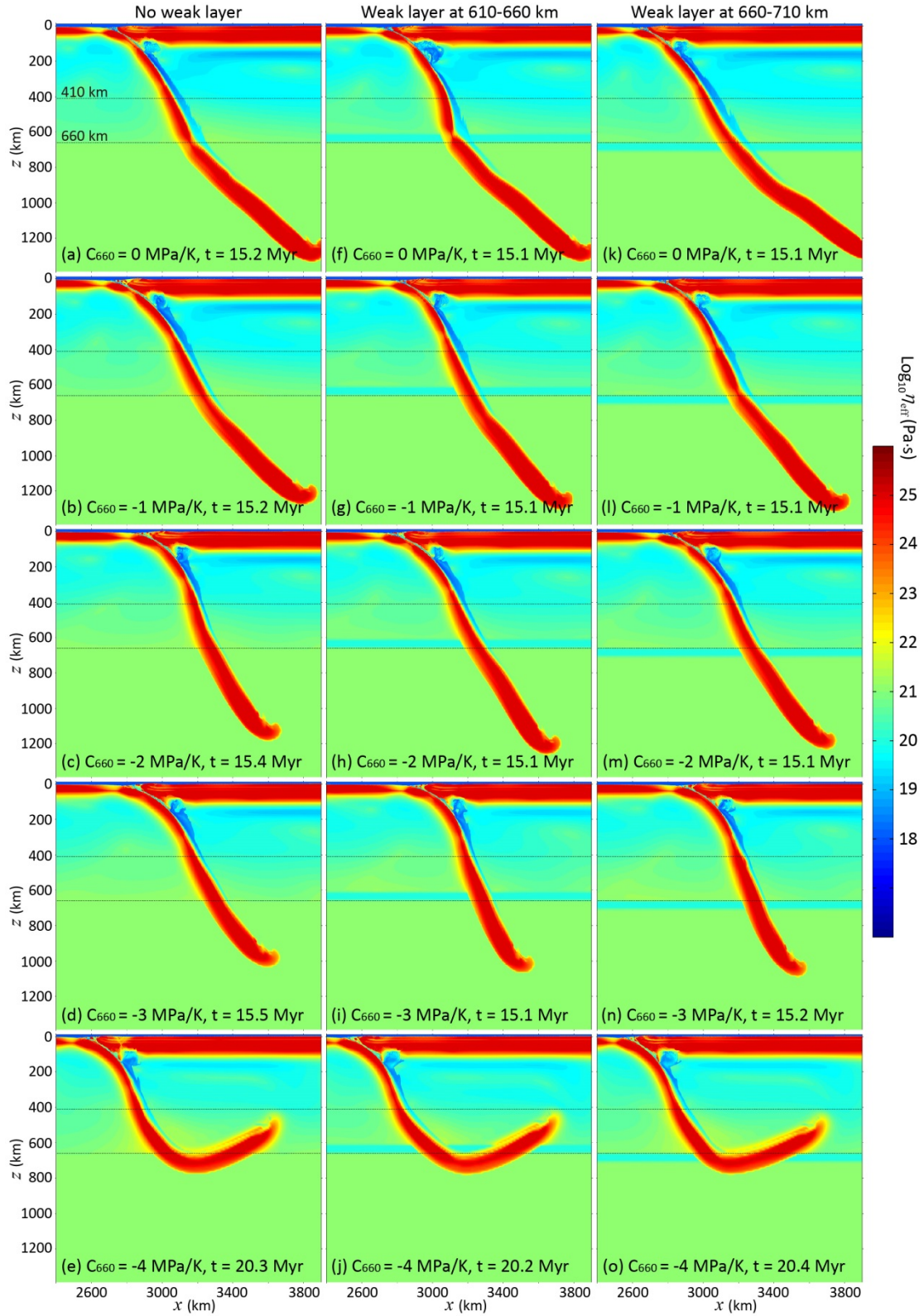
189 **Figure 3.** Model results with a constant viscosity ( $10^{22}$  Pa·s) of the lower mantle, i.e.  
 190 B-type in Figure 1e. The effects of a thin weak layer and the Clapeyron slope ( $C_{660}$ ) at  
 191 D660 are tested.

192

193 **3.3. Models with low and constant viscosity of the lower mantle ( $10^{21}$  Pa·s)**

194 In this set of models, a constant viscosity of  $10^{21}$  Pa·s is applied for the lower  
195 mantle, with an effective viscosity profile shown in Figure 1e (C-type), which  
196 represents an end-member regime with the rheologically weakest lower mantle.

197 The model results show that the sinking slab can easily penetrate the MTZ to the  
198 lower mantle, with the Clapeyron slope of  $|C_{660}| \leq 3$  MPa/K (Figure 4). It indicates  
199 that the weak lower mantle does not provide enough resistance for the slab stagnation.  
200 In contrast, with a large Clapeyron slope of  $C_{660} = -4$  MPa/K, the slab stagnates and  
201 flattens at the bottom of the MTZ, mainly due to the delay of phase transition and the  
202 consequent low density of sinking slab compared to the neighboring lower mantle,  
203 which thus provides large resistance on the subducting slab. In this set of models, the  
204 weak layer, no matter above or beneath D660, does not affect the slab morphology in  
205 the MTZ (Figure 4).



206

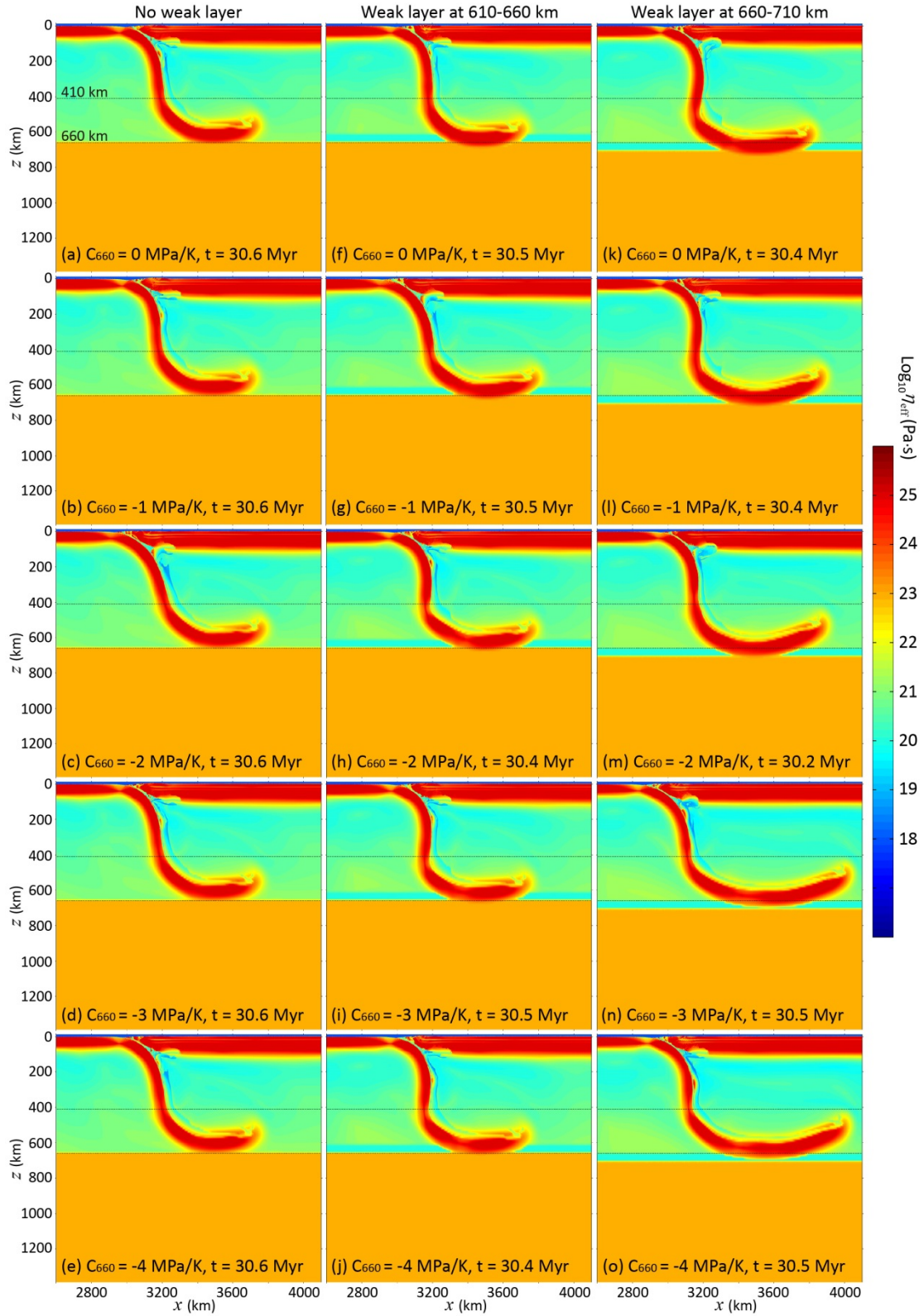
207 **Figure 4.** Model results with a constant viscosity ( $10^{21}$  Pa·s) of the lower mantle, i.e.  
 208 C-type in Figure 1e. The effects of a thin weak layer and the Clapeyron slope ( $C_{660}$ ) at  
 209 D660 are tested.

210

211 **3.4. Models with high and constant viscosity of the lower mantle ( $10^{23}$  Pa·s)**

212 In this set of models, a constant viscosity of  $10^{23}$  Pa·s is applied for the lower  
213 mantle, with an effective viscosity profile shown in Figure 1e (D-type), which  
214 represents an end-member regime with the rheologically strongest lower mantle.

215 In all the models, the slab stagnation is predicted due to the strong resistance from  
216 the lower mantle (Figure 5); however, the lengths of the flattened slab are different at  
217 the bottom of the MTZ. It shows that the weak layer above D660, i.e. at 610-660 km,  
218 does not affect the morphology of the stagnant slab in the MTZ (c.f. first and second  
219 columns of Figure 5). In contrast, the weak layer beneath D660, i.e. at 660-710 km,  
220 contributes significantly to the long slab flattening in the MTZ, which can be further  
221 promoted by a larger Clapeyron slope ( $C_{660}$ ). It indicates that the weak layer beneath  
222 D660 facilitates the sub-horizontal movement of the flat slab at the bottom of the  
223 MTZ, in cases with large resistance from the lower mantle to slab sinking.



224

225 **Figure 5.** Model results with a constant viscosity ( $10^{23}$  Pa·s) of the lower mantle, i.e.

226 D-type in Figure 1e. The effects of a thin weak layer and the Clapeyron slope ( $C_{660}$ ) at

227 D660 are tested.

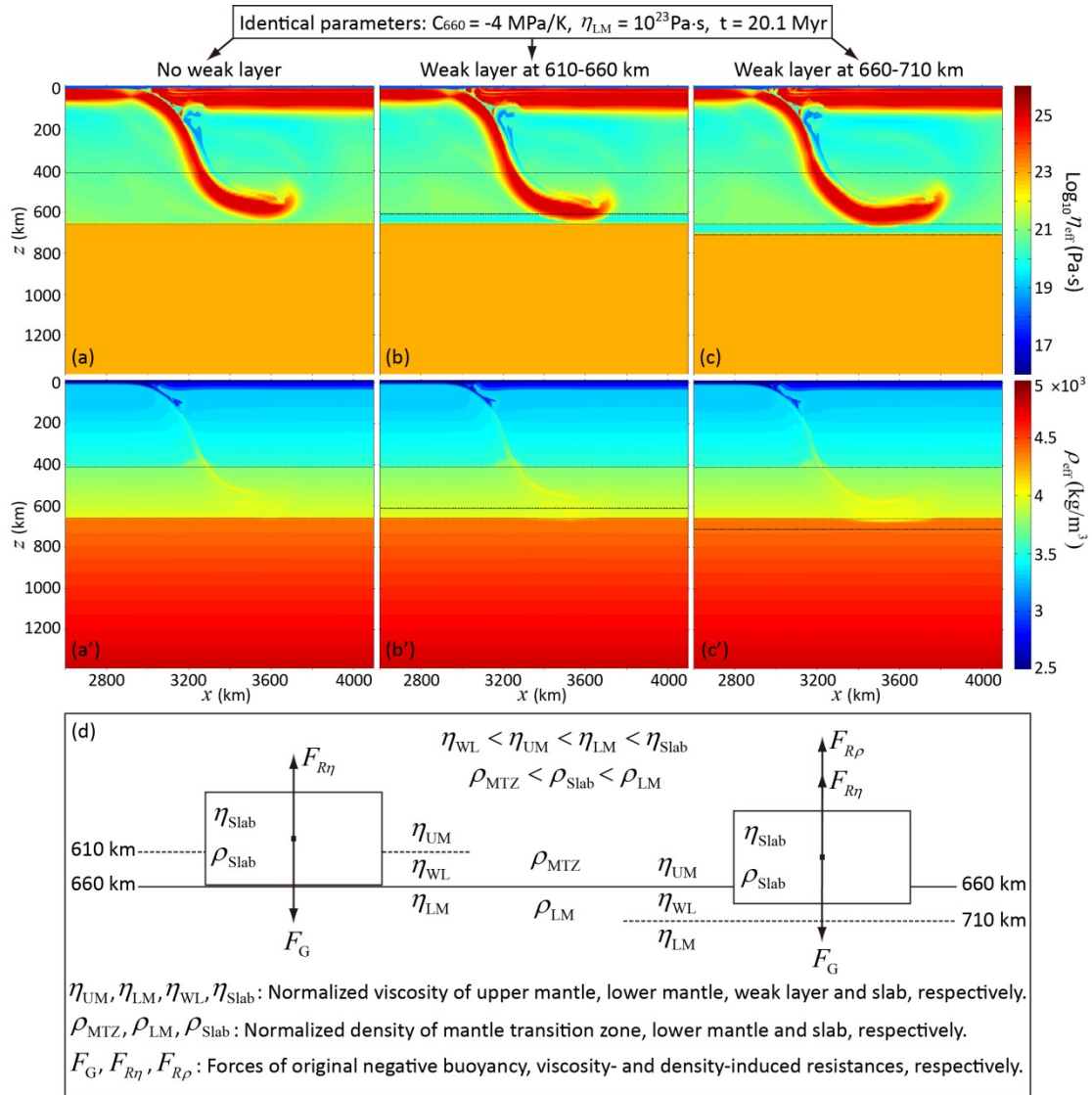
228

## 229 **4. Discussion**

### 230 **4.1. The role of a weak layer between the upper and lower mantle on slab** 231 **dynamics**

232 The systematic numerical models indicate that a thin weak layer above D660, i.e.  
233 at 610-660 km depth, has negligible effects on the subducting slab morphology in all  
234 the cases (Figures 2-5). Alternatively, if the weak layer is set at 660-710 km depth, it  
235 still does not change the general slab mode selection (penetration versus stagnation) in  
236 the MTZ. However, when the strong resistance of the lower mantle is acting on the  
237 sinking slab, the weak layer contributes to longer slab flattening at the bottom of the  
238 MTZ. The resistance could result from either a large Clapeyron slope of phase  
239 transition at D660 (e.g., Figures 2o and 3o) or a sufficient increase in the viscosity of  
240 the lower mantle (Figures 5k-n), or both (Figure 5o).

241 Figure 6 shows detailed analyses of the effects of a thin weak layer on the slab  
242 dynamics. In the regime with a weak layer at 610-660 km depth, the subducting slab  
243 sinks down, reaches the weak layer and finally touches the lower mantle (Figure 6b).  
244 Then the direct contact between the rheologically strong slab and lower mantle  
245 hinders the sub-horizontal movement of the slab along the weak layer at the bottom of  
246 the MTZ, which thus results in a similar slab mode as that without such a weak layer  
247 (Figure 6a). In an alternative regime with a weak layer at 660-710 km depth, the  
248 subducting slab arrives at D660 first. The lower density of the slab, due to the  
249 negative  $C_{660}$  and delayed phase transition, leads to slab ‘floating’ above/into the  
250 weak layer (Figures 6c, 6c’). In this case, the presence of a ‘lubrication’ layer between  
251 the rheologically strong slab and lower mantle, combining with the decreased  
252 negative buoyancy of the slab, can significantly reduce the shear resistance during the  
253 sub-horizontal slab movement (Figure 6e). It thus leads to a longer slab flattening at  
254 the bottom of the MTZ (e.g., the third column in Figure 5).



255

256 **Figure 6.** Comparison and analysis of the effects of a thin weak layer at around D660.

257 (a-c) The effective viscosity fields of the end-member models with the highest lower

258 mantle viscosity ( $10^{23} \text{ Pa}\cdot\text{s}$ ) and largest Clapeyron slope of  $C_{660} = -4 \text{ MPa/K}$ , which

259 are the same as those in Figures 5e, 5j and 5o, respectively, but at an earlier time of

260 20.1 Myr. (a'-c') The corresponding density fields of the three models (a-c),

261 respectively. (d) The force balance analyses of a simple stagnant slab in the MTZ,

262 with a weak layer at 610-660 km (left) or 660-710 km (right).

263

264 It is worth noting that the slab 'skating' along the weak layer may only exist for a

265 certain time from the initial interaction of the slab with D660. Finally, the slab may

266 sink and touch the rheologically strong lower mantle as shown in Figures 2-5, with

267 the timespan depending on the combined resistance from both the density and

268 viscosity aspects. For example, the lubrication layer is still present between the slab  
269 and strong lower mantle in the end-member models with the highest viscosity of the  
270 lower mantle ( $10^{23}$  Pa·s) and large Clapeyron slopes of  $C_{660} = -3$  or  $-4$  MPa/K  
271 (Figures 5n and 5o). However, the slab has already touched the strong lower mantle in  
272 other models with relatively low resistances (e.g., Figures 2o, 3o and 5k-m), although  
273 all the models terminate at a similar time of about 30 Myr. It indicates that both the  
274 high viscosity of the lower mantle and the large Clapeyron slope of  $C_{660}$  contribute to  
275 the sub-horizontal slab movement along the weak layer beneath D660. In addition,  
276 these two factors can compensate each other on the slab flattening at the bottom of the  
277 MTZ. For example, the weak layer at 660-710 km can only take effect with the largest  
278  $C_{660} = -4$  MPa/K in the models with an intermediate viscosity of lower mantle  
279 (Figures 2o, 3o); however, it contributes to slab flattening with lower  $C_{660}$  but a higher  
280 viscosity of lower mantle (Figures 5k-m). In addition, the weakest lower mantle  
281 prevents any effect of the weak layer on increasing slab flattening, even with the  
282 largest  $C_{660}$  (Figure 3).

283

#### 284 **4.2. Comparisons with previous models and geological implications**

285 Although a thin weak layer between the upper and lower mantle has been  
286 suggested previously based on mineral physics and geoid modeling (*Panasyuk and*  
287 *Hager, 1998; Mitrovica and Forte, 2004; Karato, 2008*), few studies have been  
288 conducted to test its effects on subduction dynamics. *Mao and Zhong (2018)*  
289 formulated a 3-D global model of mantle convection with prescribed plate and trench  
290 motions, and suggested that the weak layer beneath D660 plays a key role for slab  
291 stagnation in the MTZ, especially the large horizontal extent of stagnant slabs in the  
292 western Pacific. Further on, *Mao and Zhong (2019)* argued that an additional viscosity  
293 increase at 1000 km depth may have a similar effect as the thin weak layer beneath  
294 D660. However, the current systematic studies with more generic, pure dynamic  
295 models indicate that the effect of the weak layer may not be so crucial. It cannot  
296 change the general slab mode selection in the MTZ, i.e. penetration versus stagnation.  
297 Especially in the models with more realistic viscosities of the lower mantle (Figures

298 2-3), the weak layer can only result in a bit longer slab stagnation with a very large  
299 Clapeyron slope of  $C_{660} = -4$  MPa/K. In all the other cases, the effect of the weak  
300 layer, no matter locating above or beneath D660, is negligible on the subducting slab  
301 morphology (Figures 2-3). The detailed comparisons among models in *Mao and*  
302 *Zhong* (2018) also indicate that the weak layer does not change the slab mode from  
303 penetration to stagnation (Figure 2 and Supplementary Figure 6 in *Mao and Zhong*,  
304 2018), but does affect the length of stagnant slab, especially in the northern Honshu  
305 subduction zone. In this sense, the current 2-D generic model is not conflicting with  
306 the previous 3-D global model, but instead suggests a minor role of the thin weak  
307 layer at around D660 on the subducting slab dynamics.

308

## 309 **5. Conclusions**

310 The discontinuity (D660) at the bottom of the MTZ can strongly affect the  
311 subduction dynamics by several factors, i.e. the negative Clapeyron slope ( $C_{660} < 0$ ),  
312 the viscosity jump and the plausible presence of a thin weak layer. Their effects are  
313 systematically investigated in this study by a series of 2-D generic, pure dynamic  
314 models. The main conclusions include the following:

315 (1) The high viscosity of the lower mantle and the negative Clapeyron slope of phase  
316 transition ( $C_{660}$ ) can both contribute to slab stagnation at the bottom of the MTZ.

317 The effects of these two factors are complementary.

318 (2) A weak layer above D660, at 610-660 km depth, has negligible effect on the slab  
319 morphology in the MTZ.

320 (3) A weak layer at 660-710 km depth does not modify the slab mode selection  
321 (penetration versus stagnation) in the MTZ. However, it contributes to longer slab  
322 flattening at the bottom of the MTZ, when strong resistance of the lower mantle is  
323 acting on the sinking slab, which may be induced by either a high viscosity jump  
324 or a large Clapeyron slope.

325 (4) The role of the weak layer on slab flattening in the MTZ is strongly dependent on  
326 the lubrication effect that promotes the sub-horizontal slab movement along the  
327 weak layer at 660-710 km depth.

328 (5) Previous models without such a weak layer at around D660 are still generally  
329 valid, since the weak layer only plays a minor role in the subducting slab  
330 dynamics.

331

### 332 **Acknowledgement**

333 This work was supported by the Strategic Priority Research Program (B) of CAS  
334 (XDB18000000) and the NSFC project (41688103). Numerical simulations were run  
335 with the clusters of National Supercomputer Center in Guangzhou (Tianhe-II). *S.*  
336 *Zhong* is acknowledged for the helpful discussion. The figures of numerical models  
337 are produced by Matlab and further compiled by Adobe Illustrator. All related data  
338 will be provided in the public repository of Zenodo  
339 (<https://doi.org/10.5281/zenodo.xxxxxxx>).

340

### 341 **References**

- 342 Agrusta, R., Goes, S., & van Hunen, J. (2017). Subducting-slab transition zone interaction:  
343 stagnation, penetration and mode switches. *Earth and Planetary Science Letters*, 464, 10-23.
- 344 Billen, M. I. (2010). Slab dynamics in the transition zone. *Physics of Earth and Planetary Interior*,  
345 183, 296-308.
- 346 Čížková, H., van Hunen, J., van der Berg, A., & Vlaar, N.J. (2002). The influence of rheological  
347 weakening and yield stress on the interaction of slabs with the 670 km discontinuity. *Earth*  
348 *and Planetary Science Letters*, 199, 447-457.
- 349 Corrieu, V., Thoraval, C., & Ricard, Y. (1995). Mantle dynamics and geoid Green functions.  
350 *Geophysical Journal International*, 120, 516-523.
- 351 Cramer, F., Schmeling, H., Golabek, G. J., Duretz, T., Orendt, R., Buitter, S., et al. (2012). A  
352 comparison of numerical surface topography calculations in geodynamic modelling: An  
353 evaluation of the “sticky air” method. *Geophysical Journal International*, 189(1), 38-54.
- 354 Forte, A.M., & Peltier, W.R. (1987). Plate tectonics and aspherical Earth structure: the importance  
355 of poloidal-toroidal coupling. *Journal of Geophysical Research*, 92, 3645-3679.
- 356 Forte, A.M., & Peltier, W.R. (1991). Viscous flow models of global geophysical observables. Part  
357 1: Forward problems. *Journal of Geophysical Research*, 96, 20131-20159.
- 358 Forte, A.M., & Mitrovica, J.X. (1996). New inferences of mantle viscosity from joint inversion of  
359 long-wavelength mantle convection and post-glacial rebound data. *Geophysical Research*  
360 *letters*, 23, 1147-1150.
- 361 Forte, A.M., Quéré, S., Moucha, R., Simmons, N.A., Grand, S.P., Mitrovica, J.X., & Rowley, D.B.  
362 (2010). Joint seismic-geodynamic-mineral physical modelling of African geodynamics: a  
363 reconciliation of deep-mantle convection with surface geophysical constraints. *Earth and*  
364 *Planetary Science Letters*, 295, 329-341.

365 Gerya, T. V. (2010). Introduction to numerical geodynamic modelling. Cambridge, UK:  
366 Cambridge University Press.

367 Goes, S., Agrusta, R., van Hunen, J., & Garel, F. (2017). Subduction-transition zone interaction: a  
368 review. *Geosphere*, 13 (3), 644-664.

369 Gurnis, M., & Hager, B.H. (1988). Controls of the structure of subducted slabs. *Nature*, 335,  
370 317-321.

371 Hager, B.H., Clayton, R.W., Richards, M.A., Comer, R.P., & Dziewonski, A.M. (1985). Lower  
372 mantle heterogeneity, dynamic topography and the geoid. *Nature*, 313, 541-545.

373 Karato, S.-I. (2008). Deformation of earth materials: An introduction to the rheology of solid earth.  
374 New York: Cambridge University Press.

375 King, S., & Masters, G. (1992). An inversion for the radial viscosity structure using seismic  
376 tomography. *Geophysical Research letters*, 19, 1551-1554.

377 Lambeck, K., Johnston, P., Smither, C., & Nakada, M. (1996). Glacial rebound of the British Isles.  
378 III. Constraints on mantle viscosity. *Geophysical Journal International*, 125, 340-354.

379 Li, Z.-H., Gerya, T., & Connolly, J. A. D. (2019). Variability of subducting slab morphologies in  
380 the mantle transition zone: Insight from petrological-thermomechanical modeling.  
381 *Earth-Science Reviews*, 196, 102874.

382 Liu, H., & Leng, W. (2020). Plume-Tree Structure Induced by Low-Viscosity Layers in the Upper  
383 Mantle. *Geophysical Research Letters*, 47, e2019GL086508.

384 Mao, W., & Zhong, S. (2018). Slab stagnation due to a reduced viscosity layer beneath the mantle  
385 transition zone. *Nature Geoscience*, 11(11), 876-881.

386 Mao, W., & Zhong, S. (2019). Controls on global mantle convective structures and their  
387 comparison with seismic models. *Journal of Geophysical Research: Solid Earth*, 124,  
388 9345-9372.

389 Mitrovica, J.X., & Forte, A.M. (2004). A new inference of mantle viscosity based upon joint  
390 inversion of convection and glacial isostatic adjustment data. *Earth and Planetary Science  
391 Letters*, 225, 177-189.

392 Panasyuk, S. V., Hager, B. H. (1998). A model of transformational superplasticity in the upper  
393 mantle. *Geophysical Journal International*, 133, 741-755.

394 Ricard, Y., & Bai, W. (1991). Inferring viscosity and the 3-D density structure of the mantle from  
395 geoid, topography and plate velocities. *Geophysical Journal International*, 105, 561-572.

396 Ricard, Y., Richards, M., Lithgow-Bertelloni, C., & Le Stunff, Y. (1993). A geodynamic model of  
397 mantle density heterogeneity. *Journal of Geophysical Research*, 98, 21895-21909.

398 Schmeling, H., Babeyko, A. Y., Enns, A., Faccenna, C., Funiciello, F., Gerya, T., et al. (2008). A  
399 benchmark comparison of spontaneous subduction models - Towards a free surface. *Physics  
400 of the Earth and Planetary Interiors*, 171(1-4), 198-223.

401 Steinberger, B., & Calderwood, A.R. (2006). Models of large-scale viscous flow in the Earth's  
402 mantle with constraints from mineral physics and surface observations. *Geophysical Journal  
403 International*, 167, 1461-1481.

404 Sun, W. D., Hawkesworth, C. J., Yao, C., Zhang, C. C., Huang, R. F., Liu, X., et al. (2018).  
405 Carbonated mantle domains at the base of the Earth's transition zone. *Chemical Geology*, 478,  
406 69-75.

- 407 Tschauner, O., Huang, S., Greenberg, E., Prakapenka, V. B., Ma, C., Rossman, G. R., et al. (2018).  
408 Ice-VII inclusions in diamonds: Evidence for aqueous fluid in Earth's deep mantle. *Science*,  
409 359(6380), 1136-1139.
- 410 Turcotte, D. L., & Schubert, G. (2002). *Geodynamics*. Cambridge, UK: Cambridge University  
411 Press.
- 412 Yang, T., Moresi, L., Zhao, D., Sandiford, D., & Whittaker, J. (2018). Cenozoic lithospheric  
413 deformation in Northeast Asia and the rapidly-aging Pacific Plate. *Earth and Planetary  
414 Science Letters*, 492, 1-11.
- 415 Zhu, T. (2016). Lithospheric stress and upper mantle dynamics in mainland China due to mantle  
416 flow based on combination of global- and regional-scale seismic tomography. *Journal of  
417 Asian Earth Sciences*, 132, 103-117.
- 418

### 419 **References from the supporting information**

- 420 Bina, C. R., & Helffrich, G. (1994). Phase transition Clapeyron slopes and transition zone seismic  
421 discontinuity topography. *Journal of Geophysical Research*, 99(B8), 15,853-15,860.
- 422 Bittner, D., & Schmeling, H. (1995). Numerical modeling of melting processes and induced  
423 diapirism in the lower crust. *Geophysical Journal International*, 123, 59-70.
- 424 Clauser, C., & Huenges, E. (1995). Thermal conductivity of rocks and minerals. *Rock physics &  
425 phase relations*, 105-126.
- 426 Connolly, J. A. D. (2005). Computation of phase equilibria by linear programming: A tool for  
427 geodynamic modeling and its application to subduction zone decarbonation. *Earth and  
428 Planetary Science Letters*, 236(1-2), 524-541.
- 429 Dziewonski, A. M., & Anderson, D. L. (1981). Preliminary reference Earth model. *Physics of the  
430 Earth and Planetary Interiors*, 25(4), 297-356.
- 431 Gorczyk, W., Willner, A. P., Gerya, T. V., Connolly, J. A., & Burg, J. P. (2007). Physical controls  
432 of magmatic productivity at Pacific-type convergent margins: Numerical modelling. *Physics  
433 of the Earth and Planetary Interiors*, 163(1-4), 209-232.
- 434 Kameyama, M., Yuen, D. A., & Karato, S.-I. (1999). Thermal-mechanical effects of  
435 low-temperature plasticity (the peierls mechanism) on the deformation of viscoelastic shear  
436 zone, *Earth Planet. Science Letters*, 1-2, 159-172.
- 437 Karato, S., Riedel, M., & Yuen, D. A. (2001). Rheological structure and deformation of subducted  
438 slabs in the mantle transition zone: Implications for mantle circulation and deep earthquakes.  
439 *Physics of the Earth and Planetary Interiors*, 127, 83-108.
- 440 Karato, S., & Wu, P. (1993). Rheology of the upper mantle: A synthesis. *Science*, 260(5109),  
441 771-778.
- 442 Katz, R. F., Spiegelman, M., & Langmuir, C. H. (2003). A new parameterisation of hydrous  
443 mantle melting. *Geochemistry, Geophysics, Geosystems*, 4(9), 1073.
- 444 Kirby, S. H., & Kronenberg, A. K. (1987). Rheology of the lithosphere: selected topics. *Reviews  
445 of Geophysics*, 25, 1219-1244.
- 446 Li, Z.-H., Liu, M., & Gerya, T. (2016). Lithosphere delamination in continental collisional  
447 orogens: A systematic numerical study. *Journal of Geophysical Research: Solid Earth*, 121,  
448 5186-5211.
- 449 Ranalli, G. (1995). *Rheology of the earth, deformation and flow process in geophysics and  
450 geodynamics* (2nd ed.). London, UK: Chapman & Hall.

- 451 Rubie, D. C., & Ross, C. R. (1994). Kinetics of the olivine-spinel transformation in subducting  
452 lithosphere: Experimental constraints, and implications for deep slab processes. *Physics of the*  
453 *Earth and Planetary Interiors*, 86, 223-241.
- 454 Schmidt, M. W., & Poli, S. (1998). Experimentally based water budgets for dehydrating slabs and  
455 consequences for arc magma generation. *Earth and Planetary Science Letters*, 163(1-4),  
456 361-379.